Materials Chemistry and Physics 166 (2015) 105–115

Contents lists available at ScienceDirect

Materials Chemistry and Physics

journal homepage: www.elsevier.com/locate/matchemphys

Effects of pH and chelating agent on the NiWS phase formation in NiW/γ-Al_2O_3 HDS catalysts

C.E. Santolalla-Vargas [a], V.A. Suárez Toriello [a], J.A. de los Reyes [a, *], D.K. Cromwell [b], B. Pawelec [c], J.L.G. Fierro [c]

[a] Universidad A. Metropolitana-Iztapalapa, Área de Ingeniería Química, Av. FFCC R, Atlixco 186, Vicentina, 09340 Distrito Federal, Mexico
[b] University of New Hampshire, Department of Chemical Engineering, 207 Thompson Hall, Durham, NH 03824, USA
[c] Instituto de Catálisis y Petroleoquímica, CSIC, Cantoblanco, E-28049, Madrid, Spain

HIGHLIGHTS

- NiW/Al_2O_3 solids were prepared at different pHs and in presence of a chelating agent.
- The structure of dried and sulfided solids was characterized.
- Catalysts were tested in hydrodesulfurization of 4,6-dimethyldibenzothiophene.
- The most active NiW solid was prepared with CyDTA chelating agent at pH = 4.0.
- Most active solid exhibited the largest amount of NiWS.

GRAPHICAL ABSTRACT

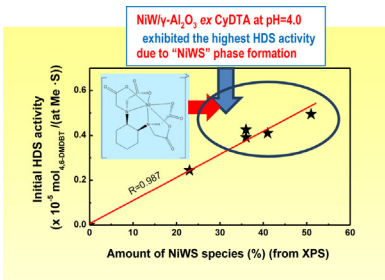

ARTICLE INFO

Article history:
Received 12 November 2014
Received in revised form
18 August 2015
Accepted 19 September 2015
Available online 1 October 2015

Keywords:
Chalcogenides
Chemical synthesis
X-ray photo-emission spectroscopy (XPS)
Surface properties
Electron microscopy (STEM, TEM and SEM)

ABSTRACT

In this article, NiW/γ-Al_2O_3 samples were prepared by consecutive impregnations of a W/γ-Al_2O_3-based catalyst with aqueous solution of nickel salt. The structural control of the nickel ion precursor in the impregnation solution was achieved by the addition of 1,2-cyclohexanediamine-N,N,N′,N′-tetraacetic acid (CyDTA) as a chelating agent. The influence of pH of this aqueous solution on the NiWS phase formation in the sulfided catalysts was investigated. Coordination structures of the Ni–CyDTA complexes were evaluated by FT-IR and DRS UV–Vis spectroscopies. Sulfided catalysts were characterized by X-ray photoelectron spectroscopy (XPS) and high resolution transmission electron microscopy (HRTEM) and tested in hydrodesulfurization (HDS) of 4,6-dimethyldibenzothiophene (4,6-DMDBT) carried out in a batch reactor at 593 K and total H_2 pressure of 55 bar. Spectroscopic characterization by DRS UV–Vis showed the predominance of the $[Ni(CyDTA)]^{2-}$ species in solution. Following the impregnation and drying steps, the $[Ni(CyDTA)]^{2-}$ complex showed no apparent changes of its structure, independent of the pH value of impregnation solution. The Ni/W/γ-Al_2O_3 catalysts *ex* $[Ni(CyDTA)]^{2-}$ complex exhibited high stability. The presence of CyDTA delayed the reduction of Ni and caused a remarkable decrease of the W-support interaction, thus increasing the formation of NiWS phase upon catalyst sulfiding. The catalyst activity–structure correlation demonstrated that the catalyst activity and selectivity is linked with formation of the most active NiWS phase having single or double WS_2 slab structures. The catalyst prepared with $[Ni(CyDTA)]^{2-}$ complex at pH of 4.0 exhibited the largest initial HDS activity, which was approximately triple compared with the CyDTA-free counterpart. For all catalysts, the HDS reaction

* Corresponding author.
E-mail address: jarh@xanum.uam.mx (J.A. de los Reyes).

http://dx.doi.org/10.1016/j.matchemphys.2015.09.033

proceeded via hydrogenation (HYD) and direct desulfurization (DDS) reaction routes, the former being the main reaction route. The addition of chelating agent led to an increase of the selectivity toward HYD route products.

1. Introduction

The research into new hydrodesulfurization (HDS) catalysts is an important topic considering the severe environmental legislation requirements for diesel fuel at present [1]. For deep HDS of diesel, the most refractory compounds are alkyl-dibenzothiophenes exhibiting planar configuration and alkyl groups in the 4- and 6-positions (4,6-DMDBT) [2]. This is because the position of the methyl groups with respect to the phenyl ring obstructs the interaction between the sulfur atom and the catalytic active site [3,4]. In the refining industry, the HDS reaction is performed usually on the γ-Al_2O_3-supported catalysts based on MoS_2 or WS_2 particles promoted by Co or Ni. However, those catalysts are not always able to perform deep HDS of alkyl-substituted DBT. Thus, the challenge is to design new catalysts, which could be more effective for deep S-removal from diesel fuel.

It is known that the steric inhibition problem of the 4,6-dimethyldibenzothiophene (4,6-DMDBT) adsorption on the active sites could be overcome through the hydrogenation of the aromatic rings, dealkylation, isomerization and/or C–C bond scission reactions [5,6]. Thus, a new catalyst needs to have enhanced hydrogenation (HYD) function. In this sense, the NiW-based catalysts have demonstrated superior hydrogenating (HYD) capacity when compared to typical hydrotreating catalysts, NiMo and CoMo. Therefore, Ni–W formulations seem to have a great potential for the deep HDS process [7]. Unfortunately, NiW/γ-Al_2O_3 catalysts present surface phenomena, which are detrimental for the nickel deposition on the WS_2 edges forming the most active so-called NiWS phase [8]. One of the factors limiting the formation of NiWS phase is a strong interaction between the support (γ-alumina) and the W atoms, as confirmed by TPR studies [9]. Thus, to obtain the NiWS phase, the W-support interaction should be lower. Moreover, the concentration of Ni in the NiWS phase should be optimized as NiS_x segregation and nickel migration might occur.

Recently, the improvement of the characteristics of the HDS sulfide catalysts was archived by the addition of a chelating agent to the impregnating solution [10–17]. The formation of Co(Ni)(II) ion-chelate complex inhibits the formation of spinel Co(Ni)-aluminate and non-active Co(Ni)MoO_4 crystalline phases [18]. Among different chelating agents studied, 1,2-cyclohexanediamine-N,N,N′,N′-tetraacetic acid (CyDTA) was determined to be the most effective [14]. Significant increases in the promotion of MoS_2 and consequently improvements in HDS activity were achieved by CyDTA addition during catalyst synthesis [11–14]. Similarly, the NiW catalyst prepared with CyDTA exhibited improvements, which were associated with a delay in the sulfidation of nickel entities and with easier sulfidation of tungsten species that favors the Ni promotion of WS_2 edges [14,15].

In literature, the role of chelating agent on the HDS activity was mainly reported for the Co(Ni)–Mo(W) samples prepared by simultaneous impregnation [10,15]. However, one might expect different interfacial coordination chemistry when consecutive impregnation method will be employed. In this sense, the study by Ohta et al. [14] demonstrated that the pre-formation of the MoS_2-like structure was necessary to induce the intrinsic promoting effect of Co on the activity of Mo/Al_2O_3. This was explained by authors as being due to the action of the chelating agent as an adjusted timing factor influencing the Co ions interaction with the MoS_2-like structure [14]. The majority of reports are focused on the effect of variation in the molar fraction of the formed metal-chelating species, according to chemical equilibrium in aqueous systems. By contrast, very few reports have investigated the effect of the solution pH [10,17] which is an important factor that controls the deprotonation of the chelating agent and electrostatic charge balance on the support surface [17]. For the NiW/γ-Al_2O_3 catalyst prepared using citric acid as chelating agent, the pH control of the nickel-citric acid solution was found to play an important role in the modulation of metal-support interactions, achieving favorable conditions for the formation of the sulfide phase and attaining important increases in the catalytic activity in the HDS of 4,6-dimethyl dibenzothiophene (4,6-DMDBT) [17]. Similar decrease of the Mo-support interaction was reported previously for the dried Mo/SiO_2–Al_2O_3 catalysts prepared with ethylenediaminetetraacetic acid (EDTA) [19].

Within this scenario, the purpose of the present investigation was to study the influence of pH and chelating agent on the characteristics of Ni/W/γ-Al_2O_3 catalysts prepared by sequential impregnation. Our objective was to maximize the formation of the NiWS phase in the sulfided Ni/W/γ-Al_2O_3 catalysts by changing the metal-support interactions. The dried samples were directly sulfided because it is known that this method increases the probability of the NiWS phase formation and it avoids decomposition of chelating agent by high calcination temperature. The aqueous solutions of the Ni salt and chelating agent, dried solids, and sulfided catalysts were characterized by different physicochemical techniques, such as FTIR, UV–Vis, TPR, XPS and HRTEM. The activity of the sulfided NiW/γ-Al_2O_3 catalysts was evaluated in the HDS of 4,6-DMDBT reaction carried out in a batch reactor at typical reaction conditions used for this reaction (T = 593 K and total hydrogen pressure of 55 bar).

2. Experimental

2.1. Catalyst preparation

It is known that wet impregnation results in the higher dispersion for the deposited phase than the incipient wetness impregnation method [20]. The W/γ-Al_2O_3 catalyst base (W nominal loading of 20 wt%) was prepared by wet impregnation of a commercial γ-Al_2O_3 (245 m^2/g, PIE = 7.0) with aqueous solution of ammonium metatungstate $(NH_4)_6H_2W_{12}O_{40}\cdot xH_2O$ (Sigma–Aldrich) at pH of 4.0. After sample drying at 393 K, the Ni was incorporated onto the W/Al_2O_3 catalyst base using appropriate amount of $Ni(NO_3)_2\cdot 6H_2O$ (98%, Sigma–Aldrich) to obtain Ni/(Ni + W) = 0.4 atomic ratio. The concentration of the ammonium metatungstate and nickel nitrate solutions were 0.12 M and 1 M, respectively. To study the effect of chelating agent and pH conditions, four Ni/W/Al_2O_3 samples were prepared at different pH by addition of 1,2-cyclohexanediamine-tetraacetic acid ($C_{14}H_{22}N_2O_8\cdot H_2O$ (99%); CyDTA) to an aqueous solutions of the nickel nitrate (CyDTA/Ni molar ratio of 1). The pH of the Ni–CyDTA solution was adjusted with the addition of ammonium hydroxide

(25% vol.) to obtain pH values of 1.7, 4.0, 5.3 and 8.2. After impregnation, all solids were dried at 393 K in air. The catalysts prepared with chelating agent will be named hereafter as $Ni_{CyDTA(x)}$/W where *x* represent the pH value of the solution. One Ni/W/γ-Al_2O_3 reference sample was prepared without chelating agent and will be named hereafter as Ni/W.

2.2. Characterization techniques

2.2.1. Diffuse reflectance ultraviolet and visible spectroscopy

Diffuse reflectance (DRS) electronic UV–Vis spectra of the starting aqueous solutions and of the granulated (0.15–0.18 mm diameter) catalysts were recorded in the absorbance mode on a Perkin Elmer Lambda 35 outfitted with a 150 mm diameter integrating sphere coated with Poly Tetra-Fluoro Ethylene (PTFE). The reflectance standard material (Spectralon 99% from Agilent Technologies) was used as reference.

2.2.2. Infrared spectroscopy

The FT-IR spectra of the initial aqueous solutions were recorded in the 200–1100 nm range on a Perkin Elmer Spectrum One equipped with universal ATR sampling accessory. Spectra were measured at room temperature at a 4 cm^{-1} resolution and the average of 30 scans per sample was used.

2.2.3. Temperature-programmed reduction

Temperature programmed reduction (TPR) of the catalysts was carried out using Altamira Instruments AMI-90 equipped with a thermal conductivity detector (TCD). Approximately 0.1 g of catalyst sample was placed in a quartz sample cell (U shaped) and then pretreated in situ at 393 K for 1 h under a pure Ar flow. The reduction of catalysts was performed from room temperature to 1273 K, under a stream of 10% H_2, employing a gas flow rate of 0.84 cm^3/s and heating rate of 10 °C/min.

2.2.4. X-ray photoelectron spectroscopy

XPS spectra of the sulfided (10% H_2S in H_2, 673 K) catalyst samples were measured at room temperature using a VG Escalab 200R spectrometer equipped with a hemispherical electron analyzer and a Mg Kα (hν = 1253.6 eV) X-ray source. The details of the XPS measurements by this spectrometer are reported elsewhere [21].

2.2.5. High-resolution transmission electron microscopy

HR-TEM images of fresh sulfided Ni/W and Ni_{CyDTA}(0.4)/W catalyst samples were collected on a JEOL 2100F microscope operating at 200 kV. The high-resolution images were captured digitally with a Gatan CCD digital camera. The images obtained were analyzed with Digital Micrograph software. The sulfided (10% H_2S in H_2, 673 K) catalysts were ultrasonically dispersed in *i*-octane at room temperature and then spread out on a holey carbon-copper microgrid. The average particle lengths and stacking of WS_2 particles were estimated from 550 nanoparticles captured in 15 images.

2.3. Activity test

The catalyst activity was evaluated in a HDS reaction of 4,6-DMDBT performed in a batch Parr reactor charged with 250 mg of freshly sulfided catalyst and 7.3×10^{-4} mol of 4,6-DMDBT (equivalent to 300 ppm of sulfur) dissolved in 100 mL of dodecane. Before reaction, the oxide precursors were sulfided *ex-situ* at 673 K for 4 h using 10% H_2S/H_2 gas mixture (1.11 cm^3/s) and then the sample was transferred to a batch reactor in the atmosphere of an inert gas. The reaction conditions were: $T = 593$ K, $P = 55$ bar of H_2 and 1200 rpm. The reaction products were analyzed by GC on a Varian CP3800 apparatus, equipped with a capillary column HP5 and a flame ionized detector, using He as carrier. The catalytic activity was expressed as the initial reaction rate (4,6-DMDBT mol transformed per second and per gram of sulfided catalyst).

3. Results and discussion

3.1. Spectroscopic characterization of an aqueous solution of $[Ni(CyDTA)]^{2-}$ complex

3.1.1. FT-IR spectroscopy

FT-IR spectroscopy was used to determine the vibrations of Ni–CyDTA(pH) complex in the aqueous solutions prepared at different pH values (1.7, 4.0, 5.3 and 8.2). Fig. 1 shows the spectra for solid and aqueous solution of CyDTA. The peaks appearing in the 1800–1200 cm^{-1} frequency region should be ascribed to the carboxylic acid [22]. In this frequency region, the spectrum for solid CyDTA (Fig. 1(a)) exhibits some vibrational frequencies corresponding to protonated carboxylic acid –COOH (1750–1700 cm^{-1}), asymmetric COO^- vibration (1655 cm^{-1} and 1584 cm^{-1}), –(C–H) CH_2 (1474 cm^{-1}), NH^+ (1368 cm^{-1}) and $-COO^-$ symmetric vibration (bands below 1460 cm^{-1}) [22–25]. Additionally, the bands corresponding to COO^- asymmetric vibration (1610 and 1571 cm^{-1}), NH^+ (1360 cm^{-1}) and COO^- symmetric vibration (bands below 1400 cm^{-1}) are observed. In comparison with this solid, the IR spectrum for the aqueous solution of CyDTA did not exhibit the protonated carboxylic acid –COOH vibrations (Fig. 1(b)). These results can be related to the deprotonation of the carboxylic acid.

Fig. 2 shows the FT-IR spectra of aqueous solution containing both CyDTA and Ni ions ($[Ni^{2+}]$ = 1 M and molar ratio Ni/CyDTA = 1), which were prepared at different pH. The spectrum for pure Ni solution (Fig. 2(a)) displays the vibration frequencies corresponding to the –OH groups and N-O at 1635, 1390 and 1340 cm^{-1}, respectively. Regardless of pH of aqueous solution, the FT-IR spectra of solutions containing both CyDTA and Ni ions (Ni–CyDTA) present vibration frequencies corresponding to asymmetric COO^- in 1590 cm^{-1} and symmetric COO^- below 1400 cm^{-1}. By comparing spectra of the solution CyDTA (Fig. 1(b)) with those for the aqueous solutions of Ni–CyDTA(pH) (Fig. 2), additional bands due to the NH^+ (1360 cm^{-1}), COOH (1750–1700 cm^{-1}) and asymmetric COO^- in 1610 and 1571 cm^{-1} vibrations could not be observed. These results suggest the bonding of Ni^{2+} ions with NH^+ and COO^- groups of the CyDTA chelating agent. Finally, all aqueous solutions of the Ni–CyDTA(pH) exhibit

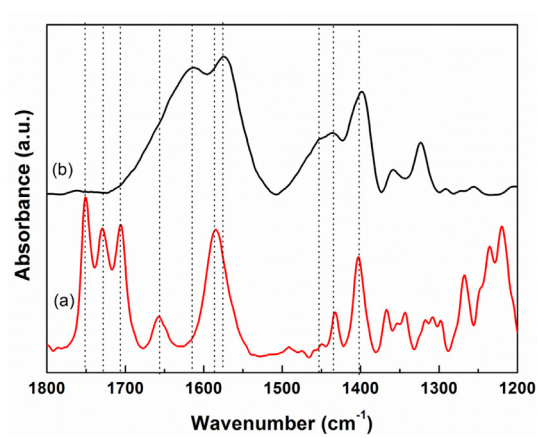

Fig. 1. FT-IR spectra of 1,2-cyclohexane diamine tetraacetic acid (CyDTA) solid (a) and in aqueous solution (b).

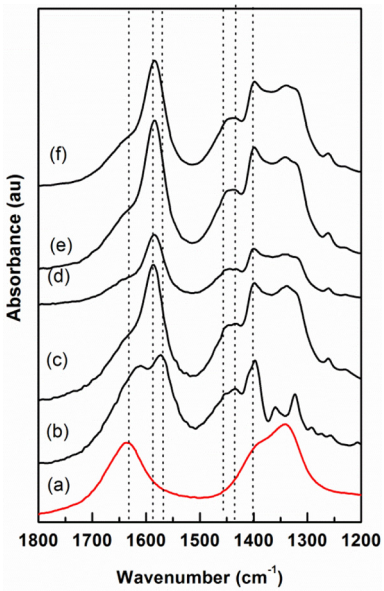

Fig. 2. FT-IR spectra of $[Ni(CyDTA)]^{2-}$ aqueous solutions ($[Ni^{2+}]$ = 1 M; Ni/CyDTA molar ratio = 1) at different pH values: (a) Ni reference sample; (b) pure CyDTA reference; (c) Ni–CyDTA(1.7), (d) Ni–CyDTA(4.0), (e) Ni–CyDTA(5.3), (f) Ni–CyDTA(8.2).

the vibrational frequency between 1590 and 1600 cm^{-1}, which could be assigned to the moieties of the five-membered rings [26,27].

3.1.2. UV–Vis spectroscopy

The UV–Vis spectra of Ni reference sample and Ni–CyDTA(pH) aqueous solutions are presented in Fig. 3. The spectrum (a) of Ni sample exhibits two bands attributable to d–d transitions. Assuming the octahedral symmetry (O_h), the bands at about 715 nm and 400 nm can be ascribed to $^3A_{2g} \rightarrow {}^3T_{1g}(F)$ and $^3A_{2g} \rightarrow {}^3T_{1g}(P)$ transitions, respectively, [28]. The band near 655 nm on a higher energy side of spin-allowed transition occurs as a result of spin-orbital coupling. The spectra of the aqueous solutions of $[Ni(CyDTA)]^{2+}$ complex exhibits four bands at 780, 620, 545 and 400 nm with a maximum absorbance at 585 nm. The bands at 780 nm and 620 nm correspond to the spin-orbital coupling. The band at 545 nm corresponds to $^3E_{1g} \rightarrow {}^3E_g$ [29] in distortion octahedral symmetry (D_{4h}) and the second band (400 nm) to $^3A_{2g} \rightarrow {}^3T_{1g}(P)$ transition in octahedral symmetry (Oh). Ni transition observed at 715 nm was shifted to 585 nm when the CyDTA was added to the solution; this shift occurs as a result of the substitution of H_2O for another stronger ligand in the spectrochemical series, in particular for carboxylic acid (COO^-) [28]. Furthermore, the absorbance between 500 and 685 nm, corresponding to distortion of octahedral symmetry (D_{4h}) in the Ni-CyDTA complex, is similar for all Ni–CyDTA solutions prepared in the entire range of pH. Erickson et al. [30] and Santini et al. [31] studied the Ni-CyDTA complex with nuclear magnetic resonance and UV–Vis, finding only one type of complex, $[Ni(CyDTA)]^{2-}$.

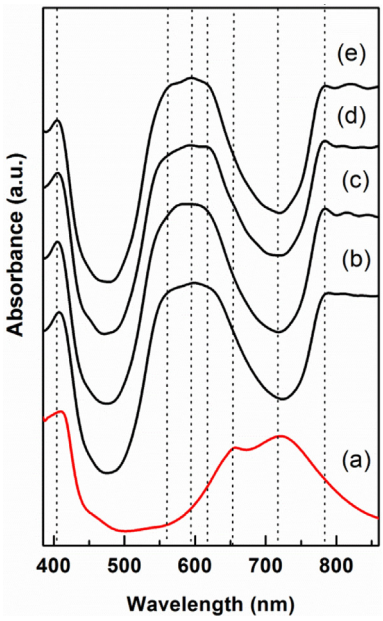

Fig. 3. UV–Vis spectra of the Ni dried samples *ex* nickel nitrate (a) and *ex* $[Ni(CyDTA)]^{2-}$ at different pH: (b) Ni–CyDTA(1.7),(c) Ni–CyDTA(4.0),(d) Ni–CyDTA(5.3), (e) Ni–CyDTA(8.2).

Summarizing, both FT-IR and DRS UV–Vis techniques indicated that irrespectively of the pH of aqueous solution, the $[Ni(CyDTA)]^{2-}$ complex has a distortional octahedral symmetry; five-membered rings and total molecular charge of −2 (see Fig. 4).

3.2. Characterization of dried Ni/W/γ-Al_2O_3 solids

3.2.1. DRS UV–Vis spectroscopy

Fig. 5 presents the DRS UV–Vis spectra of Ni/W/γ-Al_2O_3 dried samples prepared without and with chelating agent (spectra (a) and (b)–(f), respectively). The NiW sample prepared without chelating agent presents four bands at 730, 660 and 400 nm, corresponding to octahedral Ni. The band between 200 and 400 nm is attributed to $O^{2-} \rightarrow W^{6+}$ charge transfer transitions corresponding to the excitation of electrons from the valence band to the conduction band. In this interval, the presence of octahedral species can be identified between 300 and 480 nm and the tetrahedral species between 200 and 300 nm [32]. The $Ni_{CyDTA(pH)}$/W catalysts present two bands at 585 nm and 200–480 nm, corresponding to Ni in distorted octahedral symmetry (D_{4h}) and to $O^{2-} \rightarrow W^{6+}$ charge transfer transitions of W species having octahedral (Oh) and tetrahedral (Th) symmetry, respectively. This means that, regardless of pH of solution, the Ni-CyDTA complex does not modify the distorted octahedral symmetry (D_{4h}). The maximum absorbance is observed at 585 nm for the $Ni_{CyDTA(4.0)}$ and $Ni_{CyDTA(4.0)}$/W dried

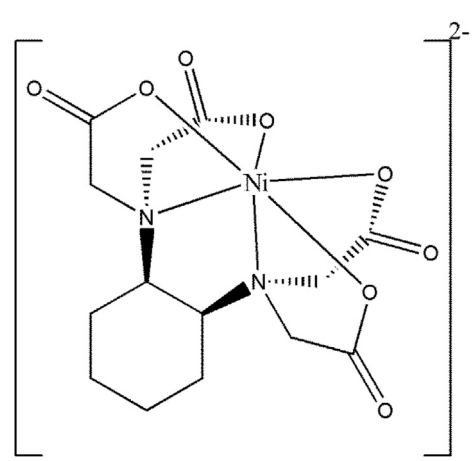

Fig. 4. Chemical structure of $[Ni(CyDTA)]^{2-}$ complex at different pH as deduced from DRS UV–Vis and FT-IR spectroscopies.

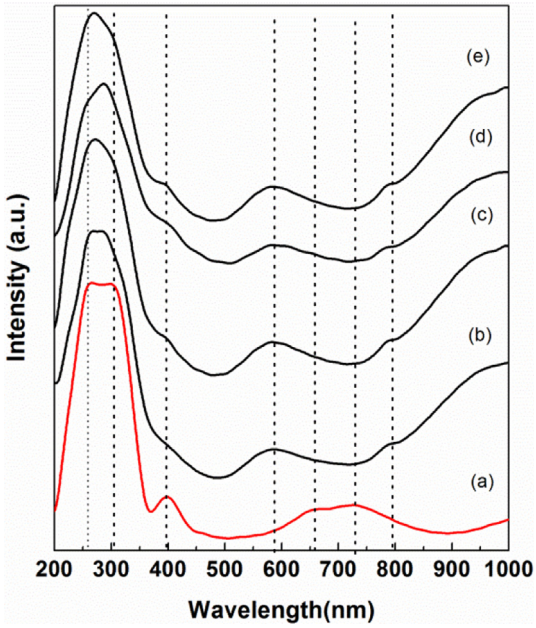

Fig. 5. DRS UV–Vis spectra of Ni/W/γ-Al_2O_3 dried samples *ex* chelating agent (CyDTA) at different pH: (a) Ni/W; (b) $Ni_{CyDTA(1.7)}$/W); (c) $Ni_{CyDTA(4.0)}$/W; (d) $Ni_{CyDTA(5.3)}$/W, and (e) $Ni_{CyDTA(8.2)}$/W.

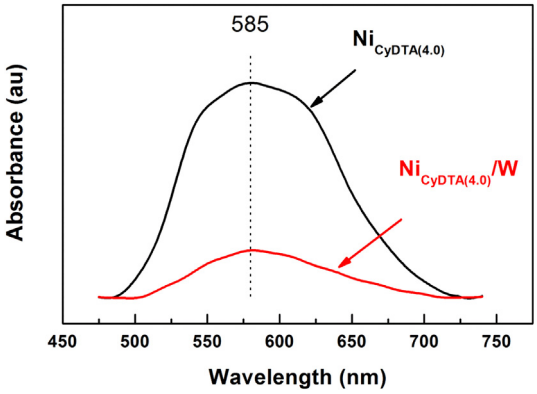

Fig. 6. DRS UV–Vis spectra of $Ni_{CyDTA(4.0)}$/W (a) and $Ni_{CyDTA(4.0)}$ (b) dried samples.

samples (Fig. 6). This observation indicates that after impregnation the coordination sphere of the Ni-CyDTA complex was not modified, discarding the possibility of "grafting" interactions. This result implies that the origin of the CyDTA effect is related to the presence of the $[Ni(CyDTA)]^{2-}$ complex.

UV–Vis spectra of the $O^{2-} \rightarrow W^{6+}$ charge transfer transition region of the dried Ni/W and $Ni_{CyDTA(pH)}$/W samples are shown in Fig. 7. As seen in this figure, the decrease in the ratio of the band intensities corresponding to the W octahedral (W_{Oh}) and tetrahedral (W_{Th}) species, W_{Oh}/W_{Th}, with an increase of the pH value occurs. This could be explained considering that during impregnation with Ni–CyDTA aqueous solution some fraction of the W species became re-dispersed on the support surface. Thus, the W_{Oh}/W_{Th} ratio could be controlled by controlling pH of the impregnating Ni–CyDTA solution.

3.2.2. Temperature-programmed reduction (TPR)

Firstly, the influence of the chelating agent on the nickel-support interaction was investigated by temperature-

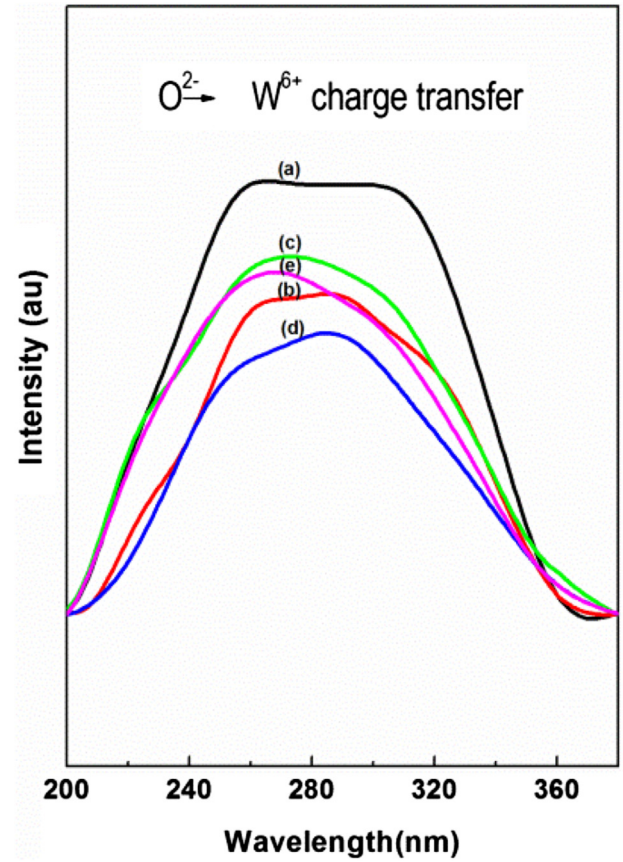

Fig. 7. DRS UV–vis spectra of $O^{2-} \rightarrow W^{6+}$ charge transfer transition region of the dried (a) Ni/W; (b) $Ni_{CyDTA(1.7)}$/W); (c) $Ni_{CyDTA(4.0)}$/W; (d) $Ni_{CyDTA(5.3)}$/W, and (e) $Ni_{CyDTA(8.2)}$/W.

programmed reduction of the monometallic Ni/γ-Al_2O_3 precursor prepared in the absence and in the presence of chelating agent. The TPR profiles of the Ni/γ-Al_2O_3 and $Ni_{CyDTA(8.0)}$/γ-Al_2O_3 samples are shown in Fig. 8. As seen in this figure, the TPR profile (a) of Ni/γ-Al_2O_3 shows one peak at 573 K corresponding to the simultaneous decomposition and reduction of nickel nitrate and two shoulders at 700 and 800 K related with Ni^{2+} species reduction in strong interaction with the γ-Al_2O_3 substrate [19]. As compared to the Ni sample prepared without chelating agent (Fig. 8(a)), the TPR profiles of the $Ni_{CyDTA(8.0)}$/γ–Al_2O_3 catalyst exhibits one peak of decomposition and reduction of $[Ni(CyDTA)]^{2-}$ complex at 723 K (TPR profile (b)). As compared with the Ni sample prepared without chelating agent, there is an important upward shift of the Ni reduction temperature (from 573 to 723 K) originated by addition of the chelating agent. The higher Ni reduction temperature strongly suggests that the $[Ni(CyDTA)]^{2-}$ complex solution could be more stable on the alumina support in comparison to $Ni(NO_3)_2$ solution.

The TPR profiles of the bimetallic NiW/γ-Al_2O_3 precursors prepared in the absence and in the presence of chelating agent are shown in Fig. 9. As seen in Fig. 9(a), the Ni/W sample prepared without CyDTA presents two reduction peaks at 563 K and 683 K, corresponding to the decomposition/reduction of nickel nitrate in weak and strong interaction with support, respectively [19]. Additionally, two shoulders can be observed at 1023 K and 1193 K, corresponding to the reduction of the different polytungstates in strong interaction with γ-Al_2O_3 [33]. The reduction profiles of $Ni_{CyDTA(pH)}$/W samples (Fig. 9(b)–(e)) exhibit two peaks: one small peak at 503 K ascribed to the reduction of nickel nitrate, and a

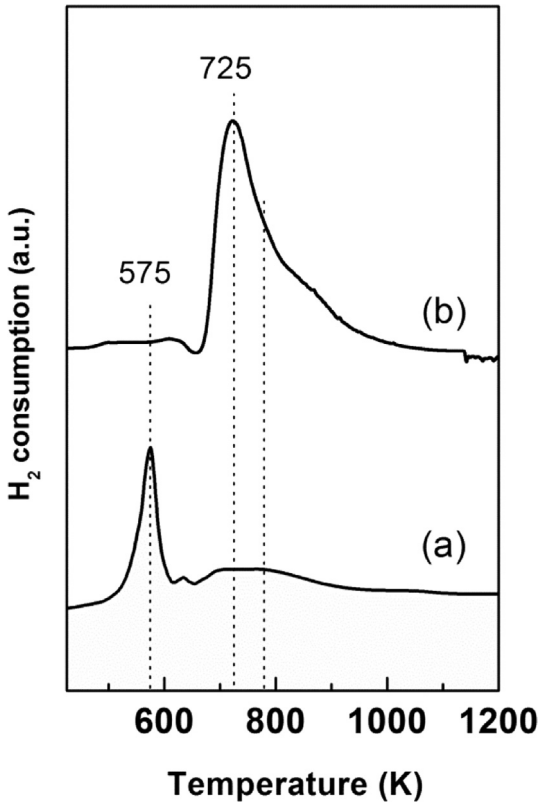

Fig. 8. TPR profiles of the dried Ni samples *ex* nickel nitrate (a) and *ex* $[Ni(CyDTA)]^{2-}$ at pH = 8.0 (b).

second one at about 723 K due to reductive decomposition of the $[Ni(CyDTA)]^{2-}$ complex.

The negative peak at 673 K is related to the decomposition of NO, NO_2 and the production of NH_3 [34]. The observed increase in the Ni reduction temperature due to the presence of CyDTA suggests the possible interaction between CyDTA and W species in W/γ-Al_2O_3. This effect was observed previously for an analogous system synthesized in the presence of EDTA [19]. Similarly to Ni/W sample, for the $Ni_{CyDTA(pH)}$/W samples, the reduction peaks above 873 K can be ascribed to the reduction of the polytungstates [33].

Considering that 50% of W species are sulfided in the temperature range 673–773 K [35], one might expect that an increase of reduction temperature of the Ni species could enhance the Ni promotion in WS_2, leading to easier formation of the NiWS phase. The observed difference between the Ni/W and $Ni_{CyDTA(pH)}$/W samples emphasize the extent to which the chelating agent can influence the reducibility of Ni oxide. The easier reduction of the samples prepared with chelating agent, as compared with the NiW sample, is attributable to chelating agent favoring the nucleation step.

3.3. Characterization of sulfided catalysts

3.3.1. X-ray photoelectron spectroscopy

To monitor the evolution of the sulfide surface species, XPS was studied in the W 4f and Ni 2p levels. As an example, the XPS spectra of W 4f emission line and fit decomposition of freshly sulfided Ni/W and $Ni_{CyDTA(4.0)}$/W samples are presented in Fig. 10. As expected, the W 4f core-level spectra of all catalysts were found rather complex, suggesting the presence of at least three species. They could be fitted satisfactorily with two sets of doublets, each one containing the W $4f_{7/2}$ and W $4f_{5/2}$ components coming from the spin–orbit

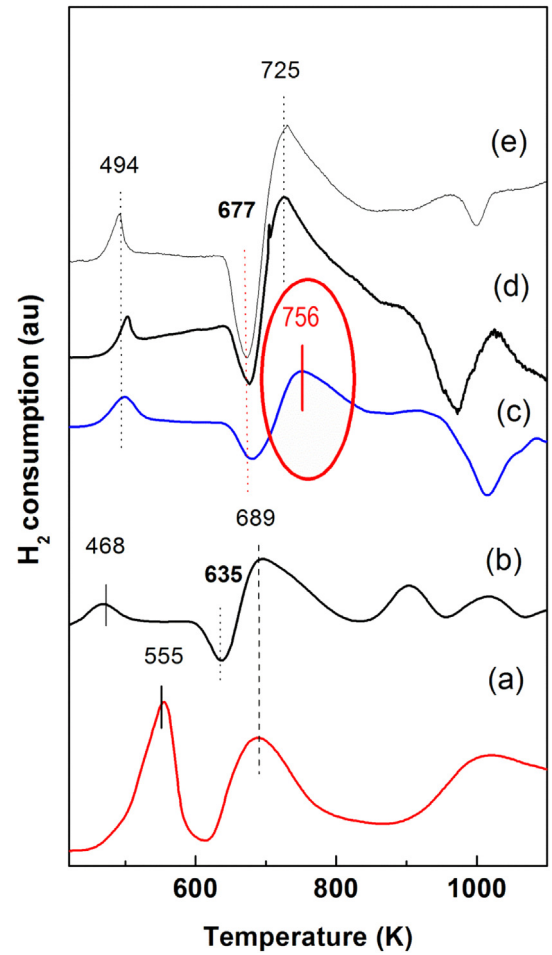

Fig. 9. TPR profiles of the dried Ni/W/γ-Al_2O_3 samples: (a) Ni/W; (b) $Ni_{CyDTA(1.7)}$/W; (c) $Ni_{CyDTA(4.0)}$/W; (d) $Ni_{CyDTA(5.3)}$/W, and (e) $Ni_{CyDTA(8.2)}$/W.

splitting. The observation of three well-resolved spin orbit split doublet peaks corresponding to W $4f_{7/2}$ and W $4f_{5/2}$ states indicates that there are three different W-species. The first doublet with W $4f_{7/2}$ and W $4f_{5/2}$ binding energy values at 32.3 and 34.4 eV, is assigned to WS_2 (W^{4+}) species [36,37] whereas the other two doublets at 34.9 and 37.1 eV, and at 35.7 and 37.8 eV are attributed to WO_xS_y (W^{5+}) and WO_x (W^{6+}) species, respectively [38,39].

Table 1 reports the relative concentration for each species. For the NiW catalyst, 66% of W species was converted to WS_2 species. This amount appears to decrease with the presence of CyDTA, changing to 58%, 47%, 53% and 49% for $Ni_{CyDTA(1.7)}$/W, $Ni_{CyDTA(4.0)}$/W, $Ni_{CyDTA(5.3)}$/W and $Ni_{CyDTA(8.2)}$/W, respectively. This result implies that the presence of CyDTA increased the interaction between W species and support or that CyDTA interacts with the W species. However, for the samples prepared with CyDTA, there is no clear indication that the pH influences the degree of sulfidation for the W species.

Fig. 11 shows the XPS spectra of the Ni 2p emission line for all fresh sulfided catalysts. As seen in this figure, all spectra show primary satellite peaks due to shake-up electrons. Since the line-shape of the Ni $2p_{3/2}$ peak, and especially its satellite, was unsymmetrical and broad, we applied an empirical method to roughly fit the curve using Gaussian/Lorentzian distributions. An example of the decomposition of Ni $2p_{3/2}$ profile made for the Ni/W sample is shown in the inlet of Fig. 11. Each Ni $2p_{3/2}$ profile was resolved in three components at 853.1, 854.4 and 855.8 eV, corresponding to highly dispersed NiS [36], NiWS [32,37] and NiO_x phases [32,37],

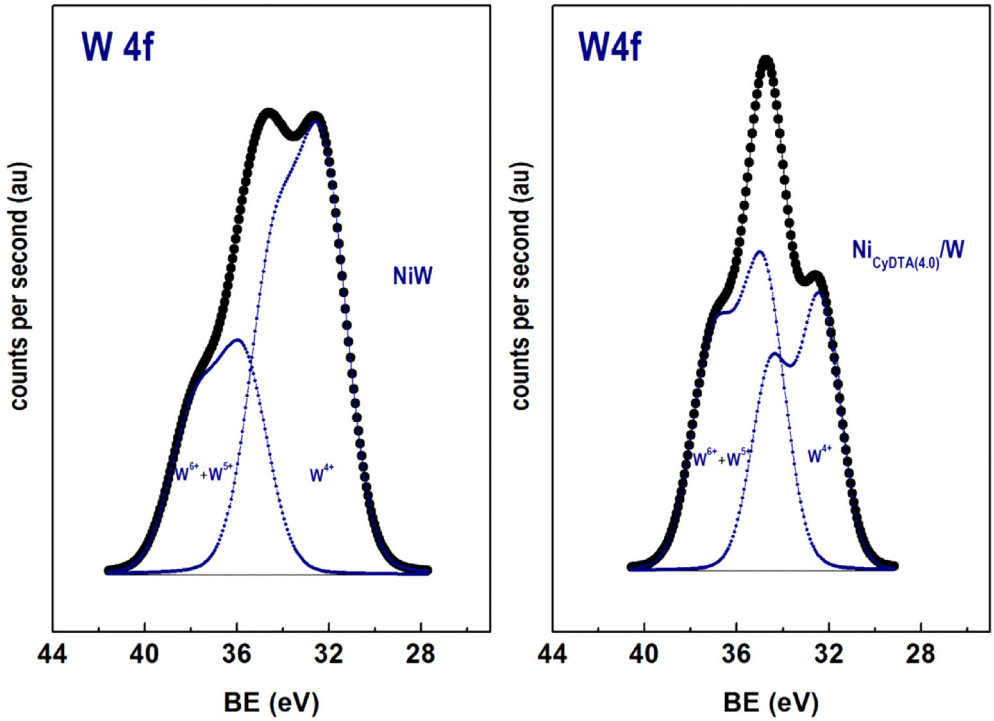

Fig. 10. W4f core-level spectra of sulfided Ni/W and $Ni_{CyDTA(4.0)}$/W samples. The experimental spectrum was deconvoluted in two W4f doublets.

Table 1
Percentage of the surface species of fresh sulfided Ni/W/Al_2O_3 catalysts (from XPS).

Catalyst	Synthesis conditions	Ni 2p core level[a]			W 4f core level[b]	
		NiS	NiWS	NiO_x	$WS_2(W^{4+})$	$WO_x + WO_xS_y(W^{6+}+W^{5+})$
Ni/W	Without CyDTA	34	23	43	66	34
$Ni_{CyDTA(1.7)}$/W	pH = 1.7; CyDTA	19	36	45	58	42
$Ni_{CyDTA(4.0)}$/W	pH = 4.0; CyDTA	13	51	36	47	53
$Ni_{CyDTA(5.3)}$/W	pH = 5.3; CyDTA	18	41	41	53	47
$Ni_{CyDTA(8.2)}$/W	pH = 8.2; CyDTA	18	36	46	49	51

[a] Ni $2p_{3/2}$ binding energy for NiS (853.1 eV), NiWS (854.4 eV) and NiO_x (855.8 eV) phases.
[b] W $4f_{7/2}$ binding energy for WS_2 (32.3 eV), WO_xS_y (34.9 eV) and WO_x (35.7 eV).

respectively. Apparently, the electronegativity of the $[Ni(CyDTA)]^{2-}$ complex has little effect on the binding energies separating satellite and main peaks of Ni $2p_{3/2}$ spectra. The BE at 853.1 eV is close to value reported in literature for bulk NiS on unsupported WS_2 (852.9 eV) [36] whereas the BE at 854.4 eV is close to value reported for NiWS species formed after sulfidation of the NiW/γ-Al_2O_3 catalysts at 673 K [40,41].

Considering the binding energy position and the relative area related to the three Ni species, the percentages of each species were determined. As seen in Table 1, the Ni/W sample exhibited 23% of the NiWS species, while the catalysts with CyDTA showed increased percentages of this species in accordance to the impregnation pH. The relative concentration of NiWS species in the $Ni_{CyDTA(1.7)}$/W, $Ni_{CyDTA(4.0)}$/W, $Ni_{CyDTA(5.3)}$/W and $Ni_{CyDTA(8.2)}$/W catalysts were 36%, 51%, 41% and 36%, respectively. From Table 2 it is evident that the proportion of NiS species is significantly lower in the samples prepared with chelating agent than in their CyDTA-free counterpart (13–19% vs. 34%) whereas the NiO_x species showed a similar presence in all catalysts. The Ni and W species surface exposure and the catalyst sulfidation degree could be deduced from Table 3 showing (Ni + W)/Al and S/(Ni + W) atomic ratios, respectively. As seen in this table, the samples prepared with CyDTA exhibit a lower Ni and W species surface exposure than the Ni/W reference sample, as deduced from the comparison of the (Ni + W)/Al atomic ratio (Table 2). Considering the TPR results (*vide supra*), this might indicate that catalyst sulfidation at 673 K led to the migration of the metal species from the support surface to its inner porous structure. Finally, there is no significant variation in the sulfidation degree of the W species, as deduced from the comparison of the S/(W + Ni) atomic ratios (Table 2).

3.3.2. High-resolution transmission electron microscopy (HRTEM)

In order to gain more insight into the changes in the dispersion of WS_2 phase induced by addition of chelating compound, the sulfided Ni/W and $Ni_{CyDTA(4.0)}$/W catalysts were investigated by HRTEM technique. Fig. 12 shows the typical dark fringes corresponding to WS_2-like structures observed on the alumina surface of both samples. For both catalysts, the measured spacing between the fringes (~0.61 nm) is consistent with the spacing (0.62 nm) of the (002) basal plane in bulk WS_2 [42]. For the Ni/W and $Ni_{CyDTA(4.0)}$/W catalysts, the average crystallite length and the stacking number are shown in Fig. 13(a) and (b), respectively. The statistical analysis of about 550 particles of the fresh sulfided Ni/W and $Ni_{CyDTA(4.0)}$/W catalysts revealed that the former catalyst possesses a little larger mean particle size than the latter (3.0 vs. 2.6 nm). The average stacking layer for $Ni_{CyDTA(4.0)}$/W was found to

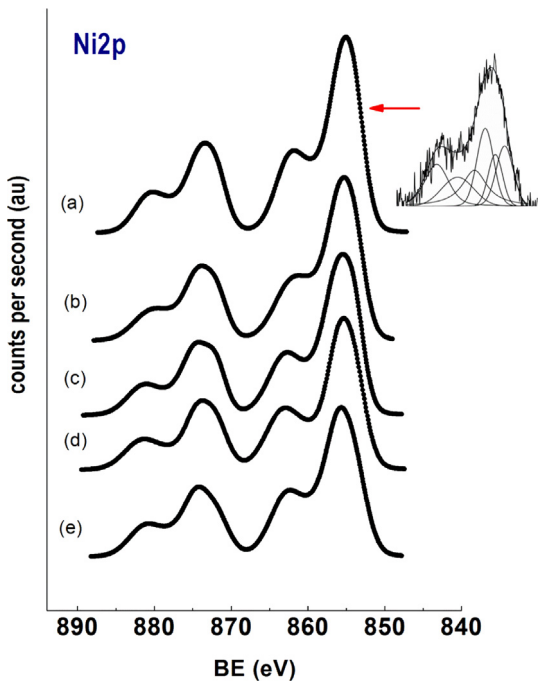

Fig. 11. X-ray photoelectron spectra of sulfided Ni/W/Al_2O_3 catalysts: (a) Ni/W; (b) $Ni_{CyDTA(1.7)}$/W; (c) $Ni_{CyDTA(4.0)}$/W; (d) $Ni_{CyDTA(5.3)}$/W, and (e) $Ni_{CyDTA(8.2)}$/W. For the Ni/W sample, deconvolution in Ni 2p emission line is shown in inset of this figure.

Table 2
W and Ni surface atomic ratios and sulfidation degree of Ni/W/Al_2O_3 sulfide catalysts (from XPS).

Sample	W/Al	Ni/Al	Ni + W/Al	S/Al	S/(W + Ni)
Ni/W	0.138	0.089	0.227	0.250	1.101
$Ni_{CyDTA(1.7)}$/W	0.072	0.056	0.128	0.117	0.914
$Ni_{CyDTA(4.0)}$/W	0.085	0.057	0.142	0.156	1.098
$Ni_{CyDTA(5.3)}$/W	0.063	0.072	0.135	0.154	1.140
$Ni_{CyDTA(8.2)}$/W	0.083	0.084	0.167	0.192	1.149

be approximately 2.3 while for the Ni/W catalyst this value was 3.2. A larger amount of NiWS (or WS_2) species having one or two slabs were formed on the sample prepared with CyDTA (60%) than on the Ni/W counterpart (35%).

3.4. Catalytic activities in the HDS of 4,6-DMDBT

The activities of the sulfided catalysts were evaluated in the HDS of 4,6-DMDBT reaction carried out in a batch reactor at T = 598 K and 55 bar of total H_2 pressure. A conventional NiW/γ-Al_2O_3 catalyst with similar metal content (14 wt% Mo and 3.8 wt% Co) was used as reference. The 4,6-DMDBT conversion at reaction time of 6 h and yield of products (at 15% of DBT conversion) are listed in

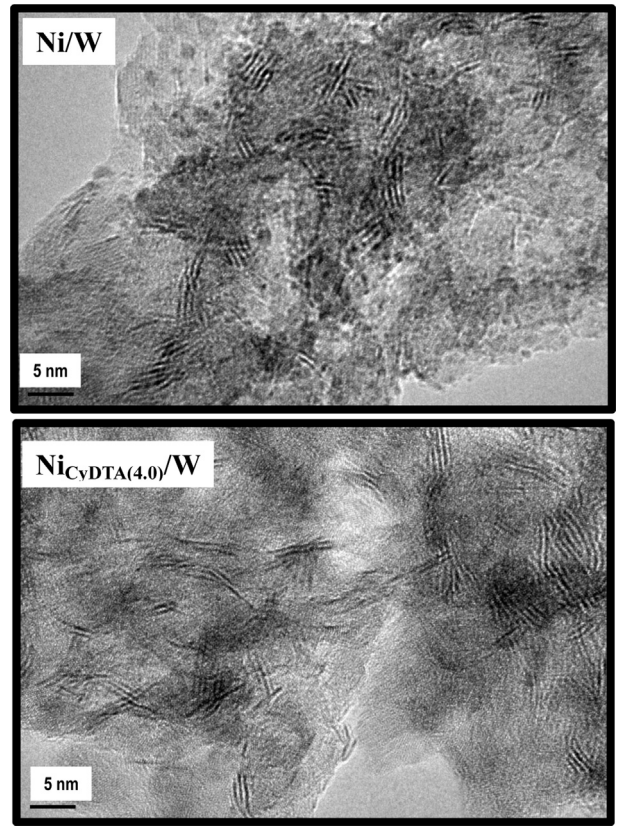

Fig. 12. HR-TEM images of the Ni/W and $Ni_{CyDTA(4.0)}$/W sulfide catalysts showing WS_2 crystallites.

Table 3. As seen, all catalysts prepared with CyDTA exhibits a larger 4,6-DMDBT conversion than Ni/W sample prepared without chelating agent. However, the influence of the pH of the aqueous solution of Ni-CyDTA complex on the 4,6-DMDBT conversion is not so clear because all catalysts prepared with chelating agent exhibits conversions in range 17.6–19.8%. This is probably because the catalysts deactivation during 6 h of reaction time. Thus, in order to clarify the effect of chelating agent, the catalyst initial activities should be compared. In Fig. 14(a) are compared the initial activities of the catalysts and their amount of the NiWS phase. As seen in this figure, the initial HDS activity and the amount of NiWS species display volcano-type curves. The most active catalyst ($Ni_{CyDTA(4.0)}$/W) exhibits the largest amount of NiWS phase (from XPS). When pH of solution is increased from 4.0 to 8.2, the initial activity decreased. At the same time, the lowering of the percentage of NiWS phase occurs. Interestingly, the initial activity of $Ni_{CyDTA(4.0)}$/W was approximately tripled compared with the NiW sample prepared without the chelating agent. Thus, it is clear that the variations in the catalytic initial activity have been related to the

Table 3
Conversion[a] and product yields (at 15% conversion) in the HDS of 4,6-DMDBT) over Ni/W/Al_2O_3 sulfide catalysts.

Catalyst	Conv.(%)	HYD reaction route			DDS reaction route	HYD/DDS ratio
		THDBT	DMCHB	DMBCH	DMBP	
Ni/W	15.8	5.8	4.4	0.8	4.8	2.29
$Ni_{CyDTA(1.7)}$/W	18.0	5.7	6.3	1.3	4.7	2.83
$Ni_{CyDTA(4.0)}$/W	17.6	6.6	5.2	1.1	4.7	2.74
$Ni_{CyDTA(5.3)}$/W	18.3	5.5	6.5	1.2	5.1	2.58
$Ni_{CyDTA(8.2)}$/W	19.8	5.9	7.2	1.3	5.4	2.67

[a] Reaction conditions were: $T = 598$ K; $P = 55$ bar; reaction time 6 h; batch reactor.

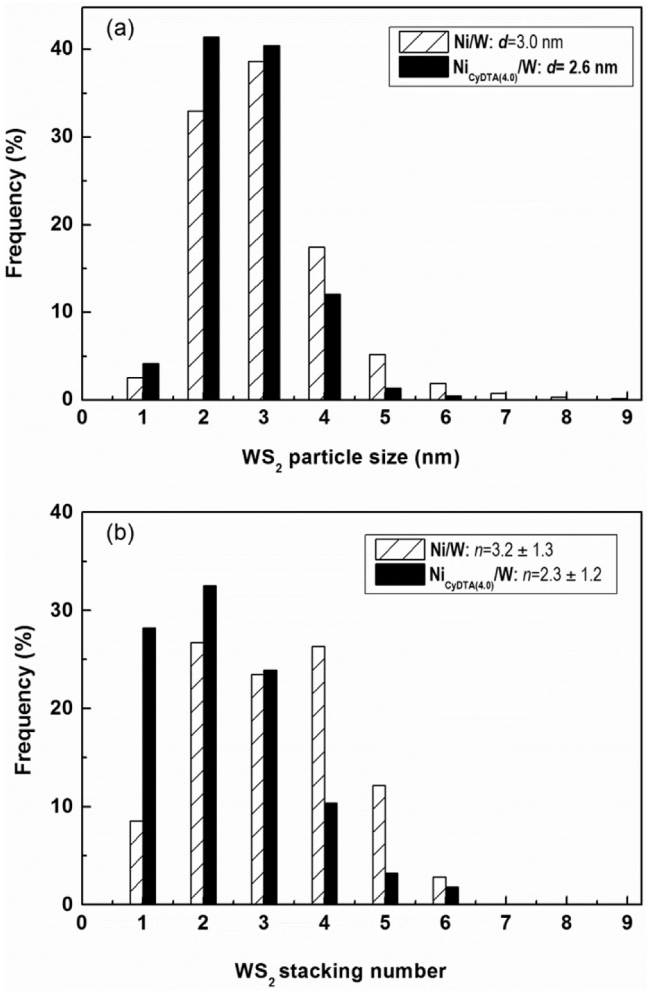

Fig. 13. WS_2 particle size and layer stacking of WS_2 slabs in the sulfided Ni/W and $Ni_{CyDTA(4.0)}$/W catalysts.

presence of the NiWS species. However, pH conditions should be controlled because the highest activity was achieved for the sample prepared at pH of 4.0.

The products detected in the HDS of 4,6-DMDBT over all catalysts studied were: 3,3′-dimethylbiphenyl (3,3-DMBP), 4,6-dimethyl-tetrahydro DBT (4,6-DMTHDBT), dimethyl-cyclohexyl benzene (DMCHB) and dimethylbicyclohexyl (DMBCH) (Table 3). Considering the products detected, the 4,6-DMDBT undergoes hydrodesulfurization via two parallel pathways (Scheme 1): (i) direct desulfurization (DDS) leading to the formation of 3,3-DMBP compound and (ii) hydrogenation (HYD) giving intermediate 4,6-DMTHDBT, which after sulfur removal through C–S bond scission is converted to DMCHB (a slow reaction) and then to DMBCH. For all catalysts studied, the 4,6-DMDBT converts mainly via the HYD pathway, as deduced from comparison of the HYD/DDS selectivity's ratio (see last column in Table 3). The use of chelating agent for the catalyst synthesis led to the enhancement of HYD route of this reaction. This is a positive effect of this synthesis method employed because the interaction between the sulfur atom and the catalytic active site requires hydrogenation prior to breaking of the C–S bond.

3.5. The catalyst activity–structure correlation

Regardless of the pH of the Ni–CyDTA solution, all catalysts prepared by consecutive impregnation of W/γ-Al_2O_3 catalyst with

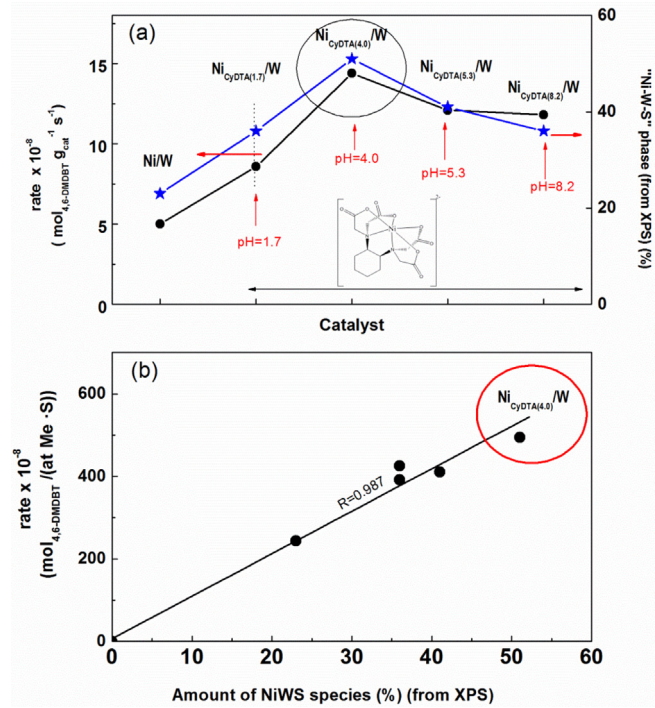

Fig. 14. (a) Comparison of the HDS initial activity and the percentage of NiWS species for the Ni/W/γ-Al_2O_3 catalysts prepared with and without CyDTA; (b) the initial HDS activity normalized to metal surface exposure vs. the amount of NiWS species (from XPS).

$[Ni(CyDTA)]^{2-}$ complex were more active in the HDS of 4,6-DMDBT than their Ni/W counterpart prepared in the absence of chelating agent. It was demonstrated that the final characteristic of the dried and sulfided Ni/W/γ-Al_2O_3 samples depends strongly on the pH of the aqueous solution of the Ni-CyDTA complex, pH = 4.0 being the optimal value. At this pH, there is a chemical equilibrium between $[Ni(CyDTA)]^{2-}$ complex located in the interface region and –OH groups of the alumina support. The role of the interface region on the adsorption of negatively charged complexes such as $[Ni–CyDTA]^{2-}$ is largely discussed in the review by Burikas et al. [43], so it will be not discussed in this work.

It has been established that W species weakly interacting with alumina surface are solubilized in high pH aqueous solutions [44]. In this work, the DRS UV–Vis study confirmed the decrease in the W_{Oh}/W_{Th} ratio of the band intensities corresponding to octahedral (W_{Oh}) and tetrahedral (W_{Th}) species upon increasing the aqueous solution pH value. Thus, one may infer that during impregnation of dried W/γ-Al_2O_3 with $[Ni(CyDTA)]^{2-}$ aqueous solution a certain fraction of the W species became re-dispersed on the support surface. In such case, one might expect the formation of tetrahedral WO_4^{2-} ions in alkaline solution while in acidic solutions the predominant species could be octahedral $W_{12}O_{42}^{12-}$ ions [33]. The lower HDS activity of the catalysts prepared at pH 5.3 and 8.2 could be explained in terms of the formation of undesired tetrahedral WO_4^{2-} moieties, which do not form the NiWS phase upon sulfiding.

A linear correlation was found between the initial HDS activity and the amount of NiWS phase formed in the fresh sulfided catalysts (Fig. 14(b)): the catalyst activity increases with an increase of the percentage of the NiWS phase formed. The most active catalyst prepared with CyDTA at pH of 4.0 developed the largest percentage of NiWS phase among the studied catalysts. Similar increase in the HDS activity was reported previously for the CoMo catalysts supported on alumina and silica-alumina, which were prepared with ethylenediaminetetraacetic acid (EDTA) and nitriloacetic acid (NTA)

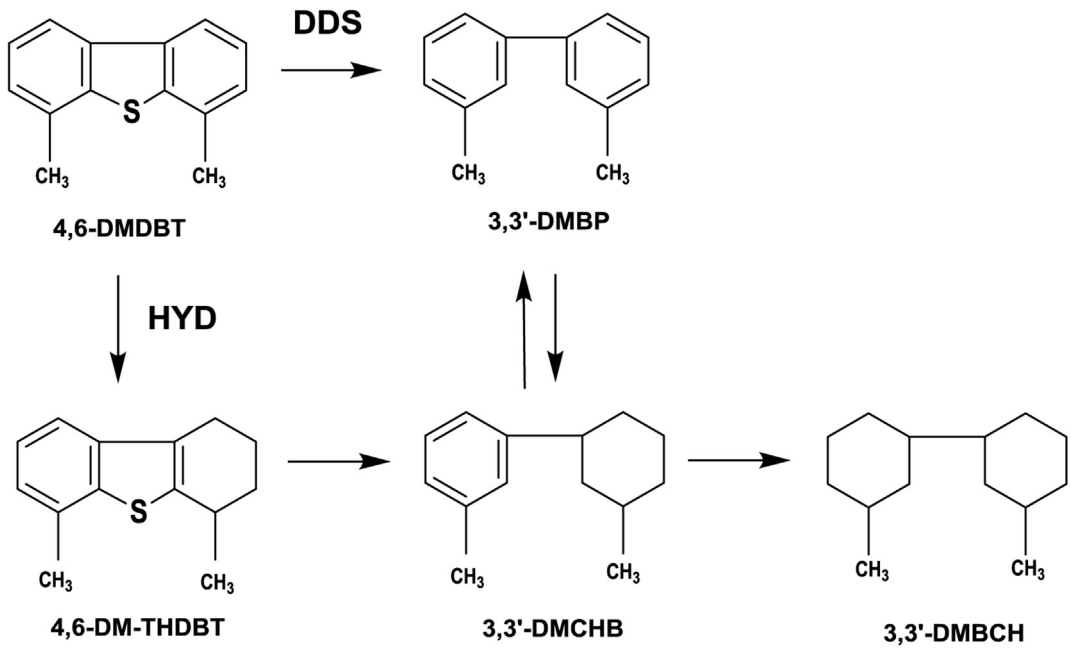

Scheme 1. Reaction scheme for HDS of 4,6-DMDBT over sulfided Ni/W/γ-Al_2O_3 catalysts *ex* chelating agent (CyDTA) at different pH.

[45] and for NiMo/SBA-15 catalysts prepared with citric acid [46]. From combined TPR and XPS characterization, the formation of NiWS phase was closely related to an enhancement of the stability of the $[Ni(CyDTA)]^{2-}$ at pH of 4.0 [43] leading to a delay in the reduction of Ni species and their simultaneous reduction with W species (Fig. 8). Additionally, the highest activity of the $Ni_{CyDTA(4.0)}$/W catalyst with respect to Ni/W sample could be also linked with its large amounts of single and double (34%) stacking WS_2 phase (>60%), as determined by statistical analysis of the number of WS_2 slabs formed on the surface of fresh sulfided catalysts (Fig. 13(b)). This is because single or double slabs displayed more edge sites in WS_2 and NiWS phases. The edge sites (named also as brim sites) exhibited metallic character [47] and, after adsorption of 4,6-DMDBT molecule on those sites, the hydrogen transfer might occur leading to transformation of this molecule via HYD reaction pathway. Indeed, in line with HRTEM data, all *ex* CyDTA catalysts exhibit a larger 4,6-DMBT transformation via HYD reaction route with respect to the CyDTA-free Ni/W catalyst (Table 3).

4. Conclusions

A significant increase in the HDS activity of Ni/W/γ-Al_2O_3 catalysts was found when the support was impregnated with the Ni-CyDTA complex at pH = 4.0. For all catalysts, the HDS reaction proceeds mainly via hydrogenation and direct desulfurization reaction routes, the former being main reaction route. The addition of chelating agent was found to enhance the selectivity toward HYD route products. The increase of HDS activity of the catalysts *ex* chelating agent was associated with an increase of the amount of active phases (NiWS species) and formation of the single or double slab WS_2 structures. After impregnation with the Ni-CYDTA complex, the redistribution and reprecipitation occur, the most appropriate impregnation being at a pH of 4.0.

Acknowledgments

C.E. Santolalla-Vargas and V.A Suarez-Toriello acknowledge financial support by CONACyT (N° 349306 and 47905). We also thank CONACyT for financial support (Grant 237857). D.K. Cromwell thanks the Hamel Center of the University of New Hampshire (USA) for funding. All authors thank Professor Gretchen Ladipus Lavine for their help in improving the quality of this work.

References

[1] EU Fuel Regulations: http://www.dieselnet.com/standards/eu/fuel.php
[2] N.K. Nag, A.V. Sapre, D.H. Broderick, B.C. Gates, Hydrodesulfurization of polycyclic aromatics catalyzed by sulfided CoO-MoO3/γ-Al2O3: the relative reactivities, J. Catal. 57 (1979) 509–512.
[3] M. Hoaulla, D.H. Broderick, A.V. Sapre, N.K. Nag, V.H.J. de Beer, B.C. Gates, H. Kwart, Hydrodesulfurization of methyl-substituted dibenzothiophenes catalyzed by sulfided Co-Mo/γ-Al2O3, J. Catal. 61 (1980) 523–527.
[4] V. Meille, E. Schulz, M. Lemaire, M. Vrinat, Hydrodesulfurization of alkyldibenzothiophenes over a NiMo/Al2O3Catalyst: kinetics and mechanism, J. Catal. 170 (1997) 29–36.
[5] T.A. Zepeda, B. Pawelec, J.L.G. Fierro, T. Halachev, Effect of Ti on the catalytic properties of CoMo/Ti(x)-HMS catalysts in the reaction of hydrodesulfurization of 4-ethyl-6-methyl dibenzothiophene, J. Catal. 242 (2006) 254–269.
[6] T.A. Zepeda, B. Pawelec, J.L.G. Fierro, T. Halachev, Removal of refractory S-containing compounds from liquid fuels on novel bifunctional CoMo/HMS catalysts modified with Ti, Appl. Catal. B Environ. 71 (2007) 223–236.
[7] S.P. Ahuja, M.L. Derrien, J.F. Le Page, Activity and selectivity of hydrotreating catalysts, Ind. Eng. Chem. Prod. Res. Dev. 9 (1970) 272–281.
[8] H. Topsøe, R. Candia, N.-Y. Topsøe, B.S. Clausen, On the state of the Co-Mo-S model, Bull. Soc. Chim. Belg. 93 (1984) 783–806.
[9] A. Spojakina, R. Palcheva, K. Jiratova, G. Tyuliev, L. Petrov, Synergism between Ni and W in the NiW/γ-Al_2O_3 hydrotreating catalysts, Catal. Lett. 104 (2005) 45–52.
[10] D. Valencia, T. Klimova, Kinetic study of NiMo/SBA-15 catalysts prepared with citric acid in hydrodesulfurization of dibenzothiophene, Catal. Commun. 21 (2012) 77–81.
[11] M. Sun, D. Nicosia, R. Prins, The effects of fluorine, phosphate and chelating agents on hydrotreating catalysts and catalysis, Catal. Today 86 (2003) 173–189.
[12] T. Shimizu, K. Hiroshima, T. Honma, T. Mochizuki, M. Yamada, Highly active hydrotreatment catalysts prepared with chelating agents, Catal. Today 45 (1998) 271–276.
[13] K. Hiroshima, T. Mochizuki, T. Honma, M. Yamada, High HDS activity of Co-Mo/Al_2O_3 modified by some chelates and their surface fine structures, Appl. Surf. Sci. 121 (1997) 433–436.
[14] Y. Ohta, T. Shimizu, T. Honma, M. Yamada, Effect of chelating agents on HDS and aromatic hydrogenation over CoMo- and NiW/Al_2O_3 Stud, Surf. Sci. Catal. 127 (1999) 161–168.
[15] K. Inamura, K. Uchikawa, S. Matsuda, Y. Akai, Preparation of active HDS catalysts by controlling the dispersion of active species, Appl. Surf. Sci. 121 (122) (1997) 468–475.

[16] G. Kishan, L. Coulier, V.H.J. de Beer, J.A.R. van Veen, J.W. Niedmantsverdriet, Sulfidation and thiophene hydrodesulfurization activity of nickel tungsten sulfide model catalysts, prepared without and with chelating agents, J. Catal. 196 (2000) 180–189.
[17] V.A. Suárez-Toriello, C.E. Santolalla-Vargas, J.A. de los Reyes, A. Vázquez-Zavala, M. Vrinat, C. Geantet, Influence of the solution pH in impregnation with citric acid and activity of Ni/W/Al_2O_3 catalysts, J. Mol. Catal. A Chem. 404 (2015) 36–46.
[18] C. Wivel, B.S. Clausen, R. Candia, S. Mørup, H. Topsøe, Mössbauer emission studies of calcined Co-Mo/Al_2O_3 catalysts: catalytic significance of Co precursors, J. Catal. 87 (1984) 497–513.
[19] K. Al-Dalama, A. Stanislaus, Temperature-programmed reduction of SiO_2–Al_2O_3 supported Ni, Mo and NiMo catalysts prepared with EDTA, Thermochim. Acta 520 (2011) 67–72.
[20] J. Vakros, C. Kordulis, On the synergy between tungsten and molybdenum in the W-incorporated CoMo/γ-Al_2O_3 hydrodesulfurization catalysts, Appl. Catal. A Gen. 217 (1–2) (2001) 287–293.
[21] R.M. Navarro, B. Pawelec, J.L.G. Fierro, P.T. Vasudevan, J.F. Cambra, P.L. Arias, Deep hydrodesulfurization of DBT and diesel fuel on supported Pt and Ir catalysts, Appl. Catal. A Gen. 137 (1996) 269–286.
[22] J. Ryczkowski, IR studies of EDTA alkaline salts interaction with the surface of inorganic oxides, Appl. Surf. Sci. 252 (2005) 813–822.
[23] D.H. Busch, C.J. Bailar, The stereochemistry of complex inorganic compounds. XVII. The stereochemistry of hexadentate ethylenediaminetetraacetic acid complexes, J. Am. Chem. Soc. 75 (1953) 4574–4575.
[24] M.L. Morris, D.H. Busch, The properties and infrared absorption spectra of complexes of cobalt(III) with pentadentate ethylenediaminetetraacetic acid and hydroxyethylethylenediaminetriacetic acid, J. Am. Chem. Soc. 78 (1956) 5178–5181.
[25] K. Nakamoto, Infrared Spectra of Inorganic and Coordination Compounds, second ed., Wiley, 1963.
[26] K. Nakamoto, Y. Morimoto, A.E. Martell, Infrared spectra of aqueous solutions. I. Metal chelate compounds of amino acids, J. Am. Chem. Soc. 83 (1961) 4528–4532.
[27] S. Belošević, M. Ćendić, A. Meetsma, Z.D. Matović, Crystal structure, configurational and DFT-NEDA analysis of nickel(II) complexes with pentadentate ed 3a-type ligands, Polyhedron 50 (2013) 473–480.
[28] F.A. Cotton, G. Wilkinson, Advanced Inorganic Chemistry. A Comprehensive Text, fourth ed., Wiley, Chichester, 1980.
[29] J.-F. Lambert, M. Hoogland, M. Che, Control of the NiII/surface interaction in the first steps of supported catalyst preparation: the interfacial coordination chemistry of $[Ni(en)_2(H_2O)_2]_2+$, Phys. Chem. B 101 (1997) 10347–10355.
[30] L.E. Erickson, D.C. Young, F.F.L. Ho, S.R. Watkins, J.B. Terrill, C.N. Reilley, Nuclear magnetic resonance studies of configuration and ligand conformation in paramagnetic octahedral complexes of nickel(II). V. Complexes of (ethylenedinitrilo)tetraacetate, (propylenedinitrilo)tetraacetate, and (trans-1,2-cyclohexylenedinitrilo)tetraacetate, Inorg. Chem. 10 (1971) 441–453.
[31] R.E. Santini, M.J. Milano, H.L. Pardue, D.W. Margerum, Swept electron beam rapid scan spectrophotometer. Qualitative aspects, Anal. Chem. 44 (1972) 826–828.
[32] J.N. Diaz de Leon, M. Picquart, L. Massin, M. Vrinat, J.A. de los Reyes, Hydrodesulfurization of sulfur refractory compounds: effect of gallium as an additive in NiWS/γ-Al_2O_3 catalysts, J. Mol. Catal. A Chem. 363 (2012) 311–321.
[33] L. Dong, Y. Hu, F. Xu, D. Lu, B. Xu, Z. Hu, Y. Chen, A study on the surface properties of ceria-supported tungsten and copper oxides, J. Phys. Chem. B 104 (2000) 78–85.
[34] S.C. Ho, T.C. Chou, The role of anion in the preparation of nickel catalyst detected by TPR and FTIR spectra, Ind, Eng. Chem. Res. 34 (1995) 2279–2284.
[35] Y. van der Meer, E.J.M. Hensen, J.A.R. van Veen, A.M. van der Kraan, Characterization and thiophene hydrodesulfurization activity of amorphous-silica–alumina-supported NiW catalysts, J. Catal. 228 (2004) 433–446.
[36] V.I. Zaikowskii, A.P. Shepelin, V.A. Burmistrov, A.N. Startsev, Yu.I. Yermakov, TEM and XPS studies of Ni/WS_2 catalysts for thiophene hydrogenolysis, React. Kinet. Catal. Lett. 25 (1984) 17–22.
[37] Z. Le, P. Afanasiev, D. Li, X. Long, M. Vrinat, Solution synthesis of the unsupported Ni-W sulfide hydrotreating catalysts, Catal. Today 130 (2008) 24–31.
[38] C. Moreno-Castilla, A.F. Pérez-Cadenas, F.J. Maldonado-Hódar, F. Carrasco-Marin, J.L.G. Fierro, Influence of carbon–oxygen surface complexes on the surface acidity of tungsten oxide catalysts supported on activated carbons, Carbon 41 (2003) 1157–1167.
[39] I.M. Szilágyi, I. Sajó, P. Király, G. Tárkányi, A.L. Tóth, A. Szabó, K. Verga-Josepovits, J. Madarász, G. Pokol, Phase transformations of ammonium tungsten bronzes, J. Therm. Anal. Calorim. 98 (2009) 707–716.
[40] H.R. Reinhoudt, E. Crezee, A.D. van Langeveld, P.J. Kooyman, J.A.R. van Veen, J.A. Moulijn, Characterization of the active phase in NiW/γ-Al_2O_3 catalysts in various stages of sulfidation with FTIR(NO) and XPS, J. Catal. 196 (2000) 315–329.
[41] L. Blanchard, J. Grimblot, J.P. Bonnelle, X-ray photoelectron spectroscopy studies on nickel-tungsten mixed sulfide catalysts, J. Catal. 98 (1986) 229–234.
[42] J. Cruz, M. Avalos-Borja, R. López Cordero, M.A. Bañares, J.L.G. Fierro, J.M. Palacios, A. López Agudo, Influence of pH of the impregnation solution on the phosphorous promotion in W/Al_2O_3 hydrotreating catalysts, Appl. Catal. A Gen. 224 (2002) 97–110.
[43] K. Bourikas, Ch. Kordulis, A. Lycourghiotis, The role of the liquid-solid interface in the preparation of supported catalysts, Catal. Rev. 48 (2006) 363–444.
[44] L. Karakonstantis, K. Bourikas, A. Lycourghiotis, Tungsten–oxo-species deposited on alumina. I. Investigation of the nature of the tungstates deposited on the interface of the γ-alumina/electrolyte solutions at various pH's, J. Catal. 162 (1996) 293–305.
[45] K. Al-Dalama, A. Stanislaus, A comparative study of the influence of chelating agents on the hydrodesulfurization (HDS) activity of alumina and silica–alumina-supported CoMo catalysts, Energy & Fuels 20 (2006) 1777–1783.
[46] T.E. Klimova, D. Valencia, J.A. Mendoza-Nieto, P. Hernandez-Hipólito, Behaviour of NiMo/SBA-15 catalysts prepared with citric acid in simultaneous hydrodesulfurization of dibenzothiophene and 4,6-dimethyldibenzothiophene, J. Catal. 304 (2013) 29–46.
[47] B. Hinneman, J.K. Norskov, H. Topsøe, A density functional study of the chemical differences between type I and type II MoS_2-based structures in hydrotreating catalysts, J. Phys. Chem. B 109 (2005) 2245–2253.